The Astrophysical Journal, 648:607–613, 2006 September 1

DIFFERENTIAL ROTATION OF ϵ ERIDANI DETECTED BY *MOST*[1]

Bryce Croll,[2] Gordon A. H. Walker,[3] Rainer Kuschnig,[2] Jaymie M. Matthews,[2] Jason F. Rowe,[2] Andrew Walker,[4] Slavek M. Rucinski,[5] Artie P. Hatzes,[6] William D. Cochran,[7] Russell M. Robb,[8] David B. Guenther,[9] Anthony F. J. Moffat,[10] Dimitar Sasselov,[11] and Werner W. Weiss[12]

Received 2006 April 3; accepted 2006 May 12

ABSTRACT

The *Microvariability and Oscillations of STars* (*MOST*) photometric satellite observed three rotations of ϵ Eri continuously in late 2005. We detected two spots ($\Delta m \sim 0.01$) at different latitudes (20.°0, 31.°5) revolving with different periods (11.35 days, 11.55 days), from which we derive a differential rotation coefficient, $k = 0.11^{+.03}_{-.02}$, in agreement with the prediction by Brown and coworkers for a young Sun-like star having roughly twice the solar angular velocity. The light curve was analyzed with the program StarSpotz, a modification of SPOTMODEL by Ribárik and coworkers. The best-fitting value for the inclination angle $i = 30^\circ \pm 3^\circ$ is compatible with inclinations already estimated for the disk ($\sim 25^\circ$) and planetary orbit (26.°2). The inclination also leads to an equatorial rotation speed of 3.42 km s^{-1} and the photometric value of $v \sin i = 1.7$ km s^{-1}. When compared with spectroscopically determined values, the photometric $v \sin i$ allows, in principle, an independent estimate of the macroturbulent velocity. Both spots would have distorted the radial velocity curve $\sim \pm 10$ m s^{-1} by the Rossiter-McLaughlin effect, which is similar to the stellar radial velocity "noise" detected by others. Details of the StarSpotz model and of the uniqueness tests that we applied in order to arrive at a best solution and realistic estimates of errors in the derived parameters are given.

Subject headings: planetary systems — stars: activity — stars: individual (ϵ Eri) — stars: late-type — stars: rotation — stars: spots

1. INTRODUCTION

ϵ Eridani ($V = 3.72$; HD 22049, HIP 16537, HR 1084) is the closest star (3.3 pc) to the Sun known to have a planetary companion (Hatzes et al. 2000). The planetary period is 6.9 yr, and Benedict et al. (2006) have estimated the planetary mass to be $1.5 M_{\rm Jup}$ and an orbital inclination of 26.°2 from *Hubble Space Telescope* (*HST*) astrometry and radial velocities. A 130 AU diameter dust ring surrounds the system inclined at $\sim 25^\circ$ (Greaves et al. 1998, 2005). An independent measurement of the stellar inclination axis from a quality light curve would provide important information on spin-orbit alignment in this system.

The star itself is K2 V and shows a high level of chromospheric activity (Gray & Baliunas 1995), consistent with a relatively young age of <1 Gyr (Soderblom & Däppen 1989). Valenti et al. (1995) made a very careful infrared Zeeman analysis of the magnetic field and concluded that some 9% of the deep photosphere of ϵ Eri is covered by a 1.44 kG field. While there is some evidence that the field may vary (Saar 1988), Valenti et al. (1995) cautioned that this may have more to do with differences in the adopted models and the relative sensitivities of optical and infrared measurements.

Several observers have found photometric variability of ϵ Eri attributable to its rotation. Vaughan et al. (1981) found a period of 11.8 days in the Ca II K-line reversal, and later, Baliunas et al. (1983) found a period of 11.3 days. Frey et al. (1991), from a photometric campaign organized in the 1988/1989 and 1989/1990 observing seasons, found five single-star spots, each of which was visible for 1 to 2 months. The spots yielded rotation periods in the range 10.0 days $< P <$ 12.3 days, with amplitudes between 0.01 and 0.03 mag. From these they estimated a differential rotational coefficient very similar to the solar value.

The *MOST* photometric satellite (Walker et al. 2003) provides continuous photometry of target stars with unprecedented precision for weeks at a time. Rucinski et al. (2004) detected a pair of spots in the *MOST* light curve of κ^1 Ceti, which had different rotation rates. In order to better decipher the spot activity and rotation of κ^1 Ceti based on the published 2003 *MOST* light curve—and two more obtained in 2004 and 2005—and to model spot distributions on other *MOST* targets, one of us (B. C.) has developed a program, StarSpotz, which is described below. The program is also expected to help in the search for spots in other stars and help define their evolution.

It has long been recognized that differential rotation and convection provide the engine for the solar dynamo (see, e.g., Ossendrijver 2003). Schau et al. (1998) found from analysis of Doppler images taken with the *Solar and Heliospheric Observatory* (*SOHO*) that the decrease of angular velocity with latitude

[1] Based on data from the *MOST* satellite, a Canadian Space Agency mission, jointly operated by Dynacon Inc., the University of Toronto Institute of Aerospace Studies, and the University of British Columbia, with the assistance of the University of Vienna.

[2] Department of Physics and Astronomy, University of British Columbia, 6224 Agricultural Road, Vancouver, BC V6T 1Z1, Canada; croll@interchange.ubc.ca, kuschnig@phas.ubc.ca, matthews@phas.ubc.ca, rowe@phas.ubc.ca.

[3] 1234 Hewlett Place, Victoria, BC V8S 4P7, Canada; gordonwa@uvic.ca.

[4] Sumus Technology Limited, Vancouver, BC, Canada; arwalker@sumusltd.com.

[5] Department of Astronomy and Astrophysics, David Dunlap Observatory, University of Toronto, P.O. Box 360, Richmond Hill, ON L4C 4Y6, Canada; rucinski@astro.utoronto.ca.

[6] Thüringer Landessternwarte Tautenburg, Sternwarte 5, D-07778 Tautenburg, Germany; artie@tls-tautenburg.de.

[7] McDonald Observatory, University of Texas, Austin, TX 78712; wdc@astro.as.utexas.edu.

[8] Department of Physics and Astronomy, P.O. Box 3055, University of Victoria, BC V8W 3P6, Canada; robb@uvic.ca.

[9] Department of Astronomy and Physics, St. Mary's University, Halifax, NS B3H 3C3, Canada; guenther@ap.stmarys.ca.

[10] Département de physique, Université de Montréal, C.P. 6128, succursale Centre-ville, Montréal, QC H3C 3J7, and Observatoire du mont Mégantic, Canada; moffat@astro.umontreal.ca.

[11] Harvard-Smithsonian Center for Astrophysics, 60 Garden Street, Cambridge, MA 02138; sasselov@cfa.harvard.edu.

[12] Institut für Astronomie, Universität Wien Türkenschanzstrasse 17, A-1180 Wien, Austria; weiss@astro.univie.ac.at.

seen at the solar surface extends with little radial variation through much of the convective layer, with a transition to nearly uniform rotation in the radiative interior through an adjustment layer called the tachocline. Angular momentum is continually redistributed in the convective envelope, which covers about one-third of the solar radius, resulting in the marked differential rotation seen at the surface (Brun & Toomre 2002).

It is assumed that, when younger, the Sun rotated more rapidly and gradually lost angular momentum through magnetic coupling to the solar wind. Calculations by Brown et al. (2004) indicate that there should be a systematic decrease of angular velocity contrast with increasing angular velocity for solar-type stars. The simultaneous detection of two or more spots at different latitudes in *MOST* light curves of solar-type stars having sufficiently short rotation periods allows us to directly measure differential rotation for stars with different ages and angular velocities—a valuable adjunct to understanding the interior rotation of the Sun and solar-type stars.

In this paper we introduce, and give details of, the program StarSpotz, and derive an inclination of the rotation axis to the line of sight, equatorial speed, $v \sin i$, and differential rotation rate for ϵ Eri.

2. THE *MOST* PHOTOMETRY

The *MOST* satellite was launched in 2003 June and is fully described by Walker et al. (2003). A 15/17.3 cm Rumak-Maksutov telescope feeds two CCDs, one for tracking and the other for science, through a single, custom, broadband filter (350–700 nm). Starlight from primary science targets ($V \leq 6$) is projected onto the science CCD as a fixed (Fabry) image of the telescope pupil covering about 1500 pixels for high photometric stability and insensitivity to detector flat-field irregularities and the effect of particle irradiation on individual pixels. The experiment was designed to detect photometric variations with periods of minutes at micromagnitude precision and does not rely on comparison stars or flat fielding for the Fabry photometry. There is no direct connection to any photometric system. Tracking jitter was dramatically reduced by early 2004 to $\sim 1''$, which led to significantly higher precision in the Fabry photometry.

The observations received from the satellite were reduced by R. K. Outlying data points generated by poor tracking or cosmic-ray hits were removed. *MOST* suffers from parasitic light, mostly earthshine, at certain orbital phases, with the amount and phase depending on the stellar coordinates, spacecraft roll, and season of the year. Data are also recorded for Fabry images from seven of the eight lenses adjacent to the target Fabry lens in order to track the stray-light background. These background signals were combined in a mean and subtracted from the target photometry. This also corrected for bias, dark, and background signals and their variations. The reductions basically followed the scheme already outlined by Rucinski et al. (2004).

MOST observed ϵ Eri from 2005 October 28 until December 3—a total of 35.7 days. More than 120,000 data points were collected, with exposure times of 20 s sampled every 25 s. Even with data points subject to high background/stray light and other outliers (South Atlantic Anomaly [SAA], bad pointing) removed, the overall duty cycle was 88%, with the longest gap being 3.5 hr. The intrinsic point-to-point precision in the unbinned light curve was 250 parts per million (ppm) rms.

For the star spot analysis, the data were binned at the *MOST* orbital period of 101.413 minutes. Figure 1 displays the full light curve with time in JD (heliocentric). Here, the point-to-point precision is 50 ppm rms. The solid line in the lower plot displays the mean background per orbit as a function of date, while the two most divergent background readings from the seven background Fabry images are shown as thin dotted and dashed lines. There is no obvious correlation between structure in the parasitic background signal and the light curve. The complete light curve can be downloaded from the *MOST* public archive.[13]

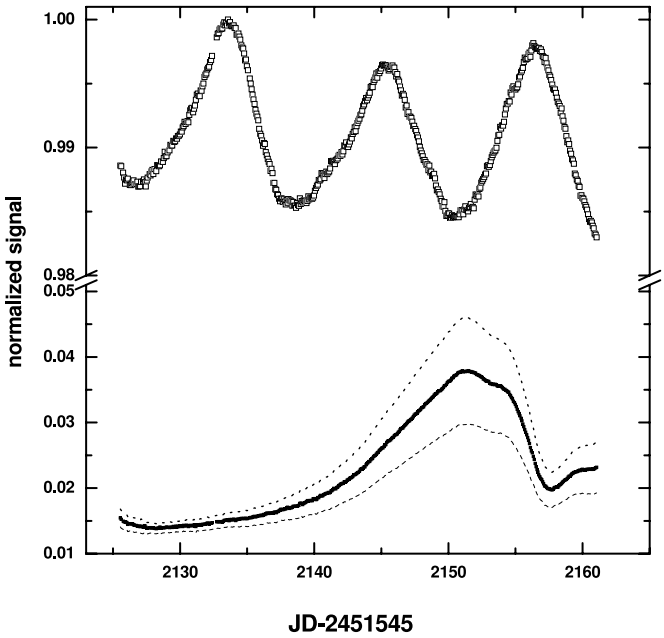

FIG. 1.—The ϵ Eri light curve observed by *MOST* in 2005. The data have been binned at the *MOST* orbital period of 101.413 minutes. Dates are heliocentric JD. The point-to-point precision is 50 ppm rms. The solid line in the lower plot displays the evolution of the mean background per orbit subtracted from the original data and derived from seven background Fabry images. The two most divergent background readings are shown by dotted and dashed lines.

A much more detailed analysis of the unbinned data of ϵ Eri has been carried out by Guenther et al. (2006), who searched for Sun-like *p*-mode oscillations with periods of minutes. In this case, parasitic light effects were aggressively removed at all satellite orbital phases according to the scheme of Reegen et al. (2006). Full details are given in Guenther et al. (2006).

3. STARSPOTZ

One of us (B. C.) has developed the program StarSpotz to return the most physically plausible configuration of star spots from an analytical fitting of models to a given light curve. The StarSpotz program is based on the SPOTMODEL program (Ribárik et al. 2003; Ribárik 2002) and is intended as a modification and improvement designed specifically to handle the nearly continuous photometry returned by *MOST*. StarSpotz includes much of the key functionality of the SPOTMODEL program, as well as improvements and other features necessary to fit the characteristics of the *MOST* light curves.

StarSpotz, like SPOTMODEL, uses a Marquardt-Levenberg nonlinear least-squares algorithm to fit the observed light curves to the analytic models of Budding (1977) or Dorren (1987). Both of these models return the theoretical light intensity as a function of time, $l_c(t)$, due to the effect of one or more nonoverlapping uniform circular spots. Extending the model to include spots with umbra/penumbra as described by Budding (1977) or Dorren (1987) has not been attempted in this first application. The two relevant stellar input parameters are given in Table 1, while the input parameters for each individual spot are listed in Table 2. The

[13] See http://www.astro.ubc.ca/MOST.

TABLE 1
StarSpotz: Stellar Input Parameters

Variable	Definition
i (deg)	Inclination of rotation axis to line of sight
U	Unspotted intensity of the star

main fitting method adapted from the SPOTMODEL program is the standard spot model (§ 3.3).

3.1. *Documentation and Release Information*

The StarSpotz program was developed in the Visual C++ environment for the Windows platform. The main StarSpotz window gives a view of the data, model, and spot configuration as it changes with the fitting process. OpenGL is used to draw the star and the spot configuration from the various view points. The StarSpotz program includes other useful functionality to return the most relevant configuration of star spots for observed photometry.[14]

3.2. *Budding and Dorren Models*

Budding (1977) estimated the drop in light intensity caused by a circular spot. He defined σ integrals for the area projected on the line of sight. The integrals are

$$\sigma_n^m = \frac{1}{\pi}\int\int_{\text{spot area}} x^m z^n dx\, dy; \tag{1}$$

σ_0^0 ($m = 0, n = 0$) represents the projected area of the spot, while σ_1^0 ($m = 0, n = 1$) represents the effect of linear limb darkening. The xyz Cartesian coordinate system orients the z-axis toward the observer. This Cartesian coordinate system can be related to the spherical polar system of longitude, λ, and latitude, β.

Budding (1977) further defined the spot-darkening function, related to the linear limb-darkening coefficient u by

$$\sigma_c = \frac{3}{3-u}\left[(1-u)\sigma_0^0 + u\sigma_1^0\right]. \tag{2}$$

The intensity of the spotted star is thus related to the unspotted intensity of the star, U, by

$$I_c(t) = U\left[1 - \sum_{j=1}^{N_{\text{spots}}}\left(1-\kappa_{\omega_j}\right)\sigma_c\left(u_j,\, \lambda_j,\, \beta_j,\, \gamma_j\right)\right], \tag{3}$$

where the j subscript represents the characteristics of the j^{th} spot. Where differential rotation is observed, longitude is an ambiguous concept and the spot location is defined better by the period, p, and epoch, E, while setting $\lambda = 0$.

The model defined by Dorren (1987) is similar to the model defined by Budding (1977). The differences between the two in terms of accuracy and computational efficiency are negligible, and thus it is left as a matter of preference for the user which model to select. Budding's model is used in this paper.

3.3. *Standard Spot Model*

The standard spot model attempts to use the analytic spot models of Budding (1977) or Dorren (1987) to fit the observed light curve. The apparent magnitude of the star, $l_o(t)$, is fitted to the theoretical magnitude, $l_c(t)$, as returned by one of the two models. The optimal configuration of star spots is obtained by minimizing the sum of squared residuals:

$$\chi^2 = \sum_{i=1}^{N}\frac{(l_{o_i} - l_{c_i})^2}{(\Delta l_{o_i})^2}. \tag{4}$$

The fitting process ends when the difference in the sum of squared residuals falls below a user-specified amount. The fitted parameters are returned with errors, as determined by the square root of the diagonal elements of the covariance matrix when the reduced χ^2 is approximately 1.0. In the case where the fitted parameters are correlated, as is often the case in photometric spot modeling, the off-diagonal elements of the covariance matrix are often nonzero, and the returned uncertainties will be underestimates.

[14] The full source code, executable, and documentation for the first and subsequent releases of this program are available at http://www.astro.ubc.ca/MOST/StarSpotz.html.

TABLE 2
StarSpotz: Spot Input Parameters

Variable	Definition
λ	Spot longitude (0° to 360°)
β	Spot latitude (−90° to 90°)
γ	Spot angular radius (0° to 90°)
p (days)	Spot period
E (HJD)	Spot epoch
κ_w	Flux ratio between spot and unspotted photosphere (0–1)
u	Linear limb-darkening coefficient (0–1)

3.4. *Uniqueness Tool*

The nonuniqueness of photometric spot modeling is a well-known limitation of the photometric method. The uniqueness tool is an attempt to define the uniqueness of a given photometric spot model solution by implementing a simple technique to search for other local minima in χ^2 space. Specifically, the tool searches for other solutions that may fit the light curve as well as or better than the given solution. In the case where the fitted parameters are correlated, the uncertainty tool returns more realistic uncertainties in the spot parameters via Monte Carlo statistics than does the standard spot model (§ 3.3).

TABLE 3
Spot Parameters for ϵ Eri from the Standard Model Analysis

Parameter	Fitted	Value[a]
Reduced χ^2	N/A	282.80
ν[b]	N/A	485
i	No	30.0
U	No	1.0000
$\kappa_{\omega 1}$, $\kappa_{\omega 2}$	No	0.220
u_1, u_2	No	0.811
E_1	Yes	2130.34 ± 0.13
p_1	Yes	11.35 ± 0.03
β_1	Yes	20.0 ± 3.2
γ_1	Yes	6.2 ± 0.13
E_2	Yes	2126.42 ± 0.11
p_2	Yes	11.55 ± 0.02
β_2	Yes	31.5 ± 2.1
γ_2	Yes	7.2 ± 0.07

[a] 1 σ errors are those returned by the standard spot model (§ 3.3), where reduced χ^2 has been scaled to 1; as the off-diagonal elements of the covariance matrix are nonzero, these errors are likely underestimates.

[b] ν is the number of binned data points minus the number of fitted parameters (eight in this case).

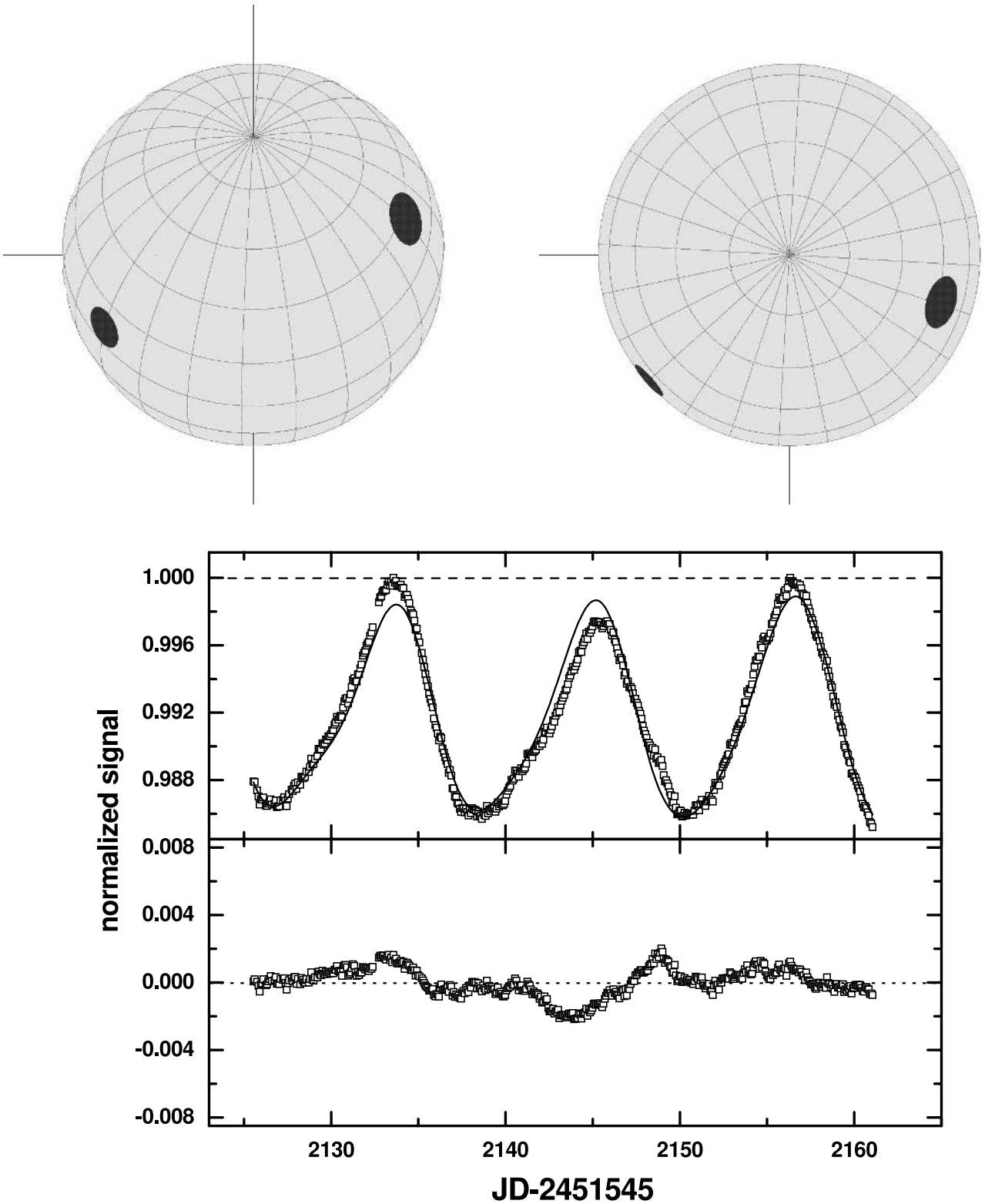

FIG. 2.—*Top:* ϵ Eri spots (Table 3) as seen from the line of sight (*left*) and the visible pole (*right*). *Middle:* The light curve of Fig. 1, with a linear trend removed. The solid line is the model from Table 3. The dashed line indicates the unspotted intensity of the star ($U = 1.0000$). *Bottom:* Residuals from the model on the same scale.

The uniqueness tool uses the user-defined best-fit model (henceforth referred to as the initial model) as its starting point while it attempts to search for other solutions that fit the light curve as well as, or better than, the initial model. The initial conditions for the standard spot model are set as a modest variation from the initial model, with the spots randomly dispersed around the star.

For instance, a one-spot solution with set U, i, κ_w, and u can be investigated by setting the initial conditions for the new period, longitude, latitude, and size of the spot as $p_{\rm new} = p_o \pm \delta p$, $\lambda_{\rm new} = \delta\lambda$, $\beta_{\rm new} = \delta\beta$, and $\gamma_{\rm new} = \delta\gamma$, where δp, $\delta\lambda$, $\delta\beta$, and $\delta\gamma$ are user-defined, appropriately sized random variables. The standard spot model fitting process is then implemented. If the parameters

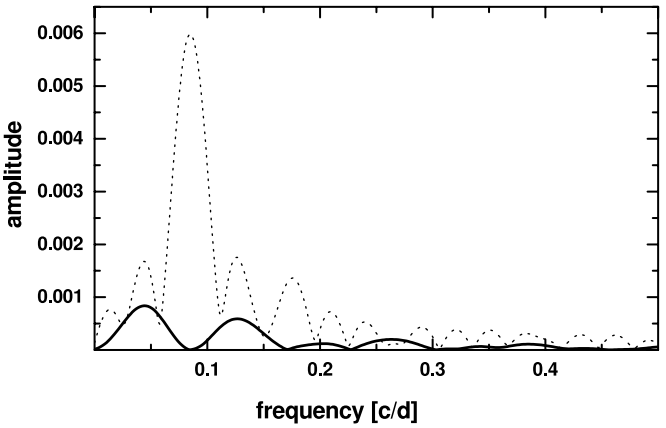

FIG. 3.—Amplitude spectra of the model (*dotted line*) of Fig. 2 and of the residuals from the model (*solid line*), demonstrating that no signal remains in the residuals over the range of rotational rates (0.088 ± 0.012 cycles day^{-1}) expected for ϵ Eri.

returned by the fit result in a sum of squared residuals that is suitably close to, or lower than, the initial model, the returned parameters are recorded.

This process is repeated as many times as is necessary to generate adequate statistics. Through this process the uniqueness of the best-fitting solution can be estimated. Solutions may be returned that fit the data as well as or better than the initial model. These alternate spot configurations can be investigated for physical plausibility.

By generating sufficient statistics, the uniqueness tool also gives better estimates of the true uncertainties in the fitted parameters. This is helpful because the effect of changing one parameter in photometric spot modeling is often closely correlated to the effect of changing an alternate parameter; as a result, the errors returned by the standard spot model (§ 3.3) are often underestimates. By generating numerous examples of the same relative configuration of star spots, Monte Carlo statistics can be generated that return more realistic uncertainties.

4. THE SPOTS ON ϵ ERI

Before analyzing the *MOST* ϵ Eri light curve shown in Figure 1, a small linear trend of 8.1328×10^{-5} day^{-1} was removed. The latter was established by normalizing the first and third maxima to 1. Since we are only interested in star spots that are expected to have rotation periods between 10 and 12 days, longer period trends, whether instrumental or intrinsic to the star, can be ignored.

Using the interactive display, it soon became clear that a two-spot model, with an inclination of $\approx 30^\circ$ provided the best fit; the StarSpotz standard model was thus applied by adopting two circular spots. The adopted linear limb-darkening coefficient, $u = 0.811$, and flux ratio between the spot and unspotted photosphere, $\kappa_\omega = 0.220$, were based on compilations of Díaz-Cordovés et al. (1995). The results of the standard model analysis are given in Table 3. The fitted spot configuration and residuals from the fit to the light curve are shown in Figure 2. Figure 3 shows the amplitude spectra of the light curve before (*dotted line*) and after (*solid line*), removing the model. The residuals obviously contain no periodicity in the expected range of rotational period and so the solution was not extended to more than two spots. We have not attempted to improve the fit using noncircular spots or by including umbra/penumbra.

4.1. ϵ *Eri Uniqueness Test*

The uniqueness test (§ 3.4) was applied to the ϵ Eri data to search for other two-spot solutions that fit the observed light curve as well as, or better than, the Table 3 model. The solution in Table 3 was used as the initial solution. The parameters that were fitted, and the range added to the Table 3 parameters for the initial condition of the fit, are given in Table 4. All other parameters are the same as in Table 3. The range in the fitted parameters as given in Table 4 was chosen by trial and error. The ranges of the parameters are believed to be sufficiently large in order to allow for all physically plausible solutions to be returned. The standard spot model was allowed to continue for 3000 iterations, or until the change in reduced χ^2 per degree of freedom fell below 10^{-21}. The returned solution was recorded if the reduced χ^2 was within $\approx$4% of the Table 3 solution (reduced $\chi^2 < 295$). This value was chosen by visual inspection, as solutions with reduced χ^2 below this value appeared to give reasonable fits to the light curve. The inclination angle was assumed to be between 25° and 35°. An additional constraint was added that the unspotted intensity of the star, U, had to be at least 1.000—the maximum signal observed.

TABLE 4
SUMMARY OF UNIQUENESS TEST INITIAL CONDITIONS FOR ϵ Eri

Parameter	Initial Value[a]	Fitted	Range or Constant Value of δ_j
i (deg).....	$i_o + \delta_i$	No	[−5.0, 5.0]
Offset.....	$U_o + \delta_U$	Yes	[−0.0015, 0.0015]
p_1, p_2 (days).....	$p_{io} + \delta_p$	Yes	[−1.0, 1.0]
E_1, E_2 (days).....	$E_{io} + \delta_E$	Yes	[−1.0, 1.0]
β_1, β_2 (deg).....	δ_β	Yes	[0, 70]
γ_1, γ_2 (deg).....	δ_γ	Yes	0.1

[a] The subscript o refers to the associated parameter in Table 3.

The uniqueness results representing all other two-spot solutions to the observed light curve are given in Table 5. We adopt solution 1 as the most appropriate. Solution 1 is identical (within the uncertainty) to our solution as given in Table 3 and presented in Figure 2. Solution 2 requires a giant spot over the visible pole, where light modulation is generated by only a slight asymmetry in the spot's location toward the observer at the epoch of minimum signal. Solutions 3 and 4 each require a huge spot covering most of the largely nonvisible hemisphere and one smaller spot in the upper hemisphere. Modulation of the light curve is generated primarily by the visible rim of the larger spot. These other solutions, although mathematically valid, seem physically implausible.

5. DISCUSSION

We consider the two-spot solution 1 from Table 5 to be the best and, as a result of the uniqueness test, we have credible errors in the various spot and stellar parameters.

5.1. *Differential Rotation*

Frey et al. (1991) extracted the differential rotation coefficient, k, from the standard expression

$$P_\beta = \frac{P_{\rm EQ}}{(1 - k \sin^2 \beta)}, \tag{5}$$

where P_β and $P_{\rm EQ}$ are the rotation periods at latitude β and on the stellar equator, respectively. In their study of ϵ Eri they determined rotation periods between 10 and 12.3 days for 12 individual spots seen over 2 years by fitting sine curves to 12 different segments of the light curve. By assuming that the spots covered the full range

TABLE 5
Two-Spot Uniqueness Solutions for ϵ Eri from StarSpotz Analysis

No.[a]	Reduced χ^{2}[b]	Inclination (i)	Offset (U)	Epoch (E)[c]	Period (p)	Latitude (β)	Size (γ)
1	282.796	30.0 ± 2.9	1.0000 ± 0.0001	2130.336 ± 0.01	11.350 ± 0.0013	20.0 ± 2.4	6.3 ± 0.4
				2126.414 ± 0.01	11.554 ± 0.0005	31.4 ± 3.4	7.3 ± 0.4
2	265.800	29.8 ± 2.9	1.4994 ± 0.0660	2127.451 ± 0.00	11.555 ± 0.0017	89.0 ± 0.3	55.5 ± 5.2
				2143.111 ± 0.01	19.269 ± 0.0147	−30.8 ± 1.6	20.4 ± 1.9
3	281.222	31.4 ± 3.0	1.0002 ± 0.0001	2130.412 ± 0.02	11.343 ± 0.0018	20.8 ± 2.5	6.0 ± 0.5
				2126.454 ± 0.01	11.552 ± 0.0011	−80.6 ± 0.3	73.6 ± 2.3
4	285.647	32.1 ± 1.0	1.0003 ± 0.0004	2130.360 ± 0.09	11.352 ± 0.0070	−79.6 ± 0.1	68.0 ± 0.9
				2126.417 ± 0.04	11.553 ± 0.0034	35.3 ± 4.0	7.0 ± 0.1

[a] Over 16,500 individual solutions with reduced $\chi^2 < 295$ were returned, all of which could be classified as one of these spot configurations. 1 σ errors are given.
[b] ν was set to be 485 for comparison with the χ^2 values in Table 3; ν properly should be 484 for the uniqueness test, as there was an additional free parameter (the unspotted intensity of the star, U).
[c] $E = \mathrm{JD} - 2,451,545$.

of β between 0° and 90° and that the period range was the result of differential rotation, they derived $k = 0.2 \pm 0.05$—a result closely similar to solar (0.19).

Using the StarSpotz program on the *MOST* light curve, we have detected two spots simultaneously, as well as a value of i. The solution provides both latitudes and rotation periods from which we derive a value of $k = 0.11^{+.03}_{-.02}$ with no ambiguity in the sign of k. The limits are set by the 1 σ range in the value of k for solution 1 of the uniqueness tests. This value of k is fairly robust and, being only half-solar, it agrees remarkably well with the prediction by Brown et al. (2004; see their Fig. 2) for a younger Sun having twice the angular velocity. In fact, from the numbers in § 5.2 the angular velocity of ϵ Eri is about a factor of 2.25 greater than solar. There is clearly a strong case to follow up these observations in another season and for other solar-type stars.

5.2. $v \sin i$ *and Equatorial Speed*

Fischer & Valenti (2005) listed values of $R_{\epsilon\,\mathrm{Eri}} = 0.76\,R_{\odot}$ and $v \sin i = 2.45$ km s^{-1} for ϵ Eri. Taking $k = 0.11$ gives $P_{\mathrm{EQ}} = 11.20$ days and an equatorial speed of 3.42 km s^{-1}, and for $i = 30°$, $v \sin i = 1.7$ km s^{-1}. Valenti et al. (1995), in their modeling for the infrared Zeeman pattern, took a value of $v \sin i = 1$ km s^{-1} (coincident with that of Marcy & Basri 1989) and a microturbulence of 1.25 km s^{-1}. It should be noted that our value of $v \sin i$ is based entirely on photometry and the estimate of $R_{\epsilon\,\mathrm{Eri}}$, making it insensitive to the magnitude of either the microturbulent or macroturbulent velocities. Fischer & Valenti (2005) quoted a median error of ~3% in $R_{\epsilon\,\mathrm{Eri}}$.

Archival spectroscopic observations from the McDonald Observatory of ϵ Eri taken at $R = 220{,}000$ are of higher resolution than those that were available to Fischer & Valenti (2005). Line profiles in ϵ Eri are narrower than in the Sun. We have tried a simple $v \sin i$ fit to the Fe I λ6256 line. Because of the low $v \sin i$, there is a trade-off between macroturbulence and rotational velocity, as mentioned in the preceding paragraph. According to Gray (1992) a G2 V star would have a macroturbulent velocity of ~4 km s^{-1} and a K2 V star would have about ~2 km s^{-1}. For a microturbulent velocity of 3 km s^{-1} the McDonald Observatory line profile implies $v \sin i = 2.5$ and 3 km s^{-1} for a microturbulent velocity of 2.5 km s^{-1}. Given the uncertainties in the value of the microturbulent velocity, the photometric value of $v \sin i = 1.7$ km s^{-1} is consistent with the spectroscopic value. A full $v \sin i$ analysis requires the right model atmosphere and appropriate Fourier analysis but, in principle, we should be able to derive an independent value for the macroturbulent velocity using the photometrically determined value of $v \sin i$.

5.3. *Rotation Axis Inclination and Possible Rossiter-McLaughlin Effect*

Our value for the inclination, $i = 30°$, of the stellar rotation axis to the line of sight is close to those determined for the planetary and disk axes but lacks an independent measurement of the azimuthal projection angle, so we cannot say whether our value of i supports a measure of spin-orbit coupling.

There was no simultaneous spectroscopic campaign accompanying the *MOST* observations, but it is interesting to note two things. First, the fractional surface area covered by the two spots is similar to the fractional surface coverage of the 1.44 kG field (Valenti et al. 1995). One cannot draw many conclusions from this, except that the active areas were of similar size at these different epochs.

The second implication of the two spots is that during transit they would have introduced distortions of the radial velocity curve by the Rossiter-McLaughlin effect (Rossiter 1924). The individual S-shaped distortion signals would have been on the order of half the revolution time of each spot, 5.5 days. Winn et al. (2005) very elegantly measured the characteristic S-shaped distortion of the radial velocity curve by the transit of the exoplanet in HD 209458. The effect arises from the imbalance in the contributions of stellar rotation to the stellar line profiles from each limb. In the case of HD 209458, the eclipse depth is ~1% and $v \sin i = 4.7$ km s^{-1}. Winn et al. (2005) detected excursions ~±40 m s^{-1}.

In the case of the spots on ϵ Eri, the individual spot intensities are ~1% and $v \sin i = 1.7$ km s^{-1}, which, by analogy with the work of Winn et al. (2005), could lead to distortions ~±10 m s^{-1}. The distortion signal would be complicated by the presence of the two spots and would essentially appear as noise in the radial velocity curve. Such a level of noise plagued early attempts to detect a planetary companion to ϵ Eri (Hatzes et al. 2000).

Our analysis of the ϵ Eri *MOST* light curve indicates that StarSpotz is a powerful tool when coupled with high-quality photometry, allowing one to determine differential rotation (when two or more spots are detected), axial inclination, equatorial rotational speed, and $v \sin i$.

The Natural Sciences and Engineering Research Council of Canada supports the research of B. C., D. B. G., J. M. M., A. F. J. M., J. F. R., S. M. R., and G. A. H. W. Additional support for A. F. J. M. comes from FCAR (Québec). R. K. and A. W. are supported by the Canadian Space Agency. W. W. W. is supported by the Austrian Space Agency and the Austrian Science Fund (P14984).

REFERENCES

Baliunas, S. L., et al. 1983, ApJ, 275, 752
Benedict, G. F., et al. 2006, AJ, in press
Brown, B. P., Browning, M. K., Brun, A. S., & Toomre, J. 2004, in Proc. *SOHO* 14 / GONG 2004 Workshop, ed. D. Danesy (ESA SP-559; Noordwijk: ESA), 341
Brun, A. S., & Toomre, J. 2002, ApJ, 570, 865
Budding, E. 1977, Ap&SS, 48, 207
Díaz-Cordovés, J., Claret, A., & Giminénez, A. 1995, A&AS, 110, 329
Dorren, J. D. 1987, ApJ, 320, 756
Fischer, D. A., & Valenti, J. 2005, ApJ, 622, 1102
Frey, G. J., Hall, D. S., Mattingly, P., Robb, S., Wood, J., Zeigler, K., & Grim, B. 1991, AJ, 102, 1813
Gray, D. F. 1992, The Observation and Analysis of Stellar Photospheres (Cambridge: Cambridge Univ. Press)
Gray, D. F., & Baliunas, S. L. 1995, ApJ, 441, 436
Greaves, J. S., et al. 1998, ApJ, 506, L133
———. 2005, ApJ, 619, L187
Guenther, D. B., et al. 2006, ApJ, submitted
Hatzes, A. P., et al. 2000, ApJ, 544, L145
Marcy, G. W., & Basri, G. 1989, ApJ, 345, 480
Ossendrijver, M. 2003, A&A Rev., 11, 287
Reegen, P., et al. 2006, MNRAS, 367, 1417
Ribárik, G. 2002, Occasional Technical Notes from Konkoly Observatory, 12 (Budapest: Konkoly Obs.), http://www.konkoly.hu/Mitteilungen/otn12.ps.Z.
Ribárik, G., Oláh, K., & Strassmeier, K. G. 2003, Astron. Nachr., 324, 202
Rossiter, R. A. 1924, ApJ, 60, 15
Rucinski, S. M., et al. 2004, PASP, 116, 1093
Saar, S. H. 1988, ApJ, 324, 441
Schau, J., et al. 1998, ApJ, 505, 390
Soderblom, D. R., & Däppen, W. 1989, ApJ, 342, 945
Valenti, J. A., Marcy, G. F., & Basri, G. 1995, ApJ, 439, 939
Vaughan, A. H., Preston, G. W., Baliunas, S. L., Hartmann, L. W., Noyes, R. W., Middelkoop, F., & Mihalas, D. 1981, ApJ, 250, 276
Walker, G. A. H., et al. 2003, PASP, 115, 1023
Winn, J. N., et al. 2005, ApJ, 631, 1215